



Quantum interference effects in titanium nitride films at low temperatures

Manosi Roy^a, Nikhil R. Mucha^a, Rahul G. Ponnamp^a, Panupong Jaipan^a, Onome Scott-Emuakpor^b, Sergey Yarmolenko^c, Alak K. Majumdar^d, Dhananjay Kumar^{a,*}

^a Department of Mechanical Engineering, North Carolina A & T State University, Greensboro, NC 27411, United States

^b Aerospace Systems Directorate (AFRL/RQTI), 1950 Fifth Street, Bldg. 18 D, Wright-Patterson AFB, OH 45433, United States

^c Department of Mechanical Engineering, Engineering Research Center, North Carolina A&T State University, Greensboro, NC 27411, United States

^d Harish-Chandra Research Institute (HRI), Allahabad 211 019, India

ARTICLE INFO

Keywords:

Titanium nitride

Resistivity minima

Quantum interference effect

ABSTRACT

Detailed electrical resistivity (ρ) measurements have been carried out in epitaxial TiN thin films in the temperature (T) range of $4 \leq T \leq 300$ K in magnetic fields from 0 to 6 T. The $\rho(T)$ data show distinct minima around 38 K, which remains unaffected by the external magnetic fields. At higher temperatures (100–300 K), the $\rho(T)$ behavior was found to be linear in agreement with classical electron-phonon interactions ($\propto T$). Below the minima, the $\rho(T)$ is unequivocally described by the quantum interference effect ($\propto -\sqrt{T}$). The value of the coefficient of the \sqrt{T} term matches well with the near-universal value.

1. Introduction

Titanium nitride (TiN) thin films are of special interest because of their excellent properties such as high melting point, wear resistance, high hardness, low electrical as well as thermal resistivity, and a very effective diffusion barrier [1–5]. Some of the applications of TiN films include microelectronic devices, cosmetic gold-colored purposes, wavelength selective transparent optical films, life extension of cutting tools, and use as a protective coating for oxidation resistance [3,4,6–8]. TiN has also emerged recently as one of the most promising alternative plasmonic materials in the visible and near-IR regions [9,10]. Our recent results have shown that TiN hard coatings can be used to increase the damping of Ti plates. The crystal structure of TiN is Rock salt with a lattice parameter of 4.24 \AA [11]. TiN belongs to the transition metals of the group IVb of the periodic table of elements. It has four valence electrons and their configuration is $3d^2 4s^2$. Ti forms electrovalent bonds with N atoms (valence electronic configuration $2s^2 2p^3$). The electronic properties of TiN are strongly dependent on the microstructures and crystallinity of TiN films [3,4,12].

The objective of this research work is to develop a fundamental understanding of the nature of electron transport in epitaxial TiN films. TiN is intrinsically non-magnetic. Structurally high-quality TiN films were grown in-situ on c-plane sapphire substrates using a pulsed laser deposition method. The emphasis of our study is to understand the physical phenomena responsible for the low temperature resistivity minima in metallic TiN thin films. The phenomenon of resistivity

minima in metallic systems at low temperatures is a very interesting subject [13–18]. The study of resistivity minima started with the observation of minima in non-magnetic crystalline metals containing very diluted magnetic impurities [18]. Later, this phenomenon was also observed in non-magnetic crystalline systems with a high concentration of magnetic impurities. Subsequently, the resistivity minima have been observed in ferromagnetic and non-ferromagnetic amorphous and crystalline alloys. The uniqueness of the present work stems from the observation of resistivity minimum in non-magnetic stoichiometric TiN thin film system containing no intentional magnetic or non-magnetic impurities. TiN films were grown purposely with higher resistivity ($\sim 300 \mu\Omega\text{cm}$) to see more pronounced resistance minima at substantially higher temperatures. These values of resistivity for TiN films is almost and order of magnitude higher than bulk TiN resistivity values [19]. It should be noted that the resistivity minima that we have observed here in TiN is of a very general nature. Other groups have also observed resistance minima in TiN films [20]. Although the focus of the work in this reference is primarily epitaxial growth of TiN films, the $\rho(T)$ data for TiN films in that paper have clear minima. However, if the TiN film is semiconducting, the resistivity minima is not observed as recently reported by Lin et al. TiN films were reported by Lin et al. to be semiconducting in the entire temperature range of 4.2–300 K [20].

2. Experimental

TiN thin films were deposited by a pulsed laser deposition (PLD)

* Corresponding author.

E-mail address: dkumar@ncat.edu (D. Kumar).

<https://doi.org/10.1016/j.tsf.2019.05.005>

Received 29 October 2018; Received in revised form 5 April 2019; Accepted 3 May 2019

Available online 06 May 2019

0040-6090/© 2019 Elsevier B.V. All rights reserved.

method using a 99.99% pure TiN target and c-Plane (0001) Al_2O_3 as substrates. The size of the substrates used was $10\text{ mm} \times 6\text{ mm} \times 0.5\text{ mm}$. Substrates were cleaned by acetone and methanol in a sonicating bath for 10–15 min to remove any impurities from the substrate. After mounting the substrate, the chamber was pumped down for 5–6 h to get to the desired vacuum pressure of $\sim 133.32 \times 10^{-6}\text{ Pa}$. Substrate temperature was kept constant at 773 K for every deposition and a target-substrate distance of $\sim 7\text{ cm}$ was maintained to ensure the uniform deposition of the film [21–23]. An excimer laser (Coherent Complex pro) with krypton fluoride (KrF) radiation (wavelength 248 nm, pulse duration 30 ns) was used during the PLD experiments. The target was continuously rotated and rastered with a frequency of 10 Hz to achieve a stable material flux and to avoid any uneven holes at a single point on the target surface. A total of 4500 number of pulses were used, which resulted a 150 nm thickness of the film. The energy density of the laser beam falling on the target was 3 J/cm^2 . The thicknesses of the TiN films were measured using X-ray reflectivity (XRR) method and surface profilometer. X-ray Diffractometer (Bruker D8) with $\text{CuK}\alpha$ radiation was used to investigate the structural property of all the samples using θ -2 θ , rocking curve and ϕ -scan. The in-plane electrical resistance versus temperature measurements were carried out using a four-probe method using the Quantum Design physical property measurement system (PPMS) via AC transport (ACT) option. The current passed during electrical measurements was 1 mA. The magnetic field applied was perpendicular to the direction of the current flow. The $\rho(T)$ data were recorded using different temperature intervals: (a) every 10 K from 300 to 70 K, (b) every 1 K from 70 to 10 K and (c) at every 0.25 K from 20 to 4 K to save experimental time, measure T_{min} accurately, and to have more data points in the region of interest.

2.1. Theoretical background of resistivity minima

The low temperature $\rho(T)$ data were analyzed using various theories of resistance minima, described briefly here [18,24–27]. In crystalline pure metals and dilute alloys, the electrical properties are well described by the quasi-classical Boltzmann transport equation (BTE) where the resistance monotonically decreases with decrease in temperature [23,28]. When electrons have mean free path (λ) of the order of lattice constants, electrical transport via BTE fails at low temperatures due to the weak localization of electrons giving rise to the Coulomb anomaly. The theory of localization was developed by several authors a few decades ago; some of the seminal work on the theory of localization can be found in the following papers [13,24–27]. If the electrical resistivity of a metallic system is of the order of $150\text{--}200\ \mu\Omega\text{cm}$ or more, the mean free path of electrons is as small as the lattice constants and so the electrons do not move in classical trajectories. They are more appropriately thought of as diffusing from site to site. The conductivity (σ) is related to the diffusion constant (D) through the generalized Einstein equation, $\sigma = e^2 D N(E_F)$, where $N(E_F)$ is the density of states at the Fermi level and e is the electronic charge. In this situation, interference of electron waves scattered by impurity or defect sites cannot be ignored; rather it becomes a necessity. It has been shown by Altshuler and Aronov [24] that quantum considerations enhance the probability of back scattering if the impurity scattering is elastic. So, there is an additional contribution to the resistivity over and above that given by the BTE. At finite temperatures, inelastic electron-phonon (e-p) scattering comes into play and tends to destroy the phase coherence and hence the additional resistivity. So, the resistivity decreases with the increase in temperature. As the resistivity finally increases due to the e-p scattering itself, a minimum in the resistivity versus temperature curve is observed [12].

Localization considers only single electrons and could take place even if electrons did not interact with each other. By contrast, the Coulomb anomaly or e-e interaction [28] arises from the interaction of one conduction electron with another in the presence of multiple elastic

scattering processes. Here also we consider interference effects between the wave-functions of the two electrons which tends to suppress the additional resistivity, which in turn decreases with increasing temperature as $\sim \sqrt{T}$. In Kondo effect also ρ decreases with increasing temperature but the temperature dependence is different. Very dilute low-resistive alloys, like CuMn, AuFe, AgMn, etc. show resistance minima where, ρ well below the minima is given by $\rho(T) = \rho_0 + J \ln T$ [18,29]. If the exchange energy J is negative, the magnetic resistivity increases as T is lowered. Historically, W. J. de Haas, J de Boer, and G. J. van den Berg were the first to discover resistance minima in pure Au but no physical interpretation was given [30–33]. Such minima at T_m were later ascribed by Kondo to the localized magnetic impurities that are far apart and interact by polarizing the conduction electrons [18]. He had shown that the anomalously large scattering probability by magnetic ions is due to the dynamic nature of scattering by the exchange coupling and the sharpness of the Fermi surface. Most importantly, the Kondo minima disappear in magnetic fields; both T_m and the depth of minima depend on impurity concentration.

3. Results and discussion

Fig. 1 shows the X-ray diffraction (XRD) pattern of a TiN thin film deposited on c-plane sapphire substrate at $500\text{ }^\circ\text{C}$; only (111) and (222) TiN peaks are seen suggesting the film is highly textured with respect to $\langle 111 \rangle$ orientation. Shown in the inset of Fig. 1 is an XRD rocking curve with 0.072 degree of full width half maxima value. This indicates perfect alignment of $\langle 111 \rangle$ TiN planes parallel to c-planes of sapphire substrate. The direction and sharpness of in-plane alignment was determined using reciprocal space mapping of (200) TiN diffraction peak observed in azimuthal scans (ϕ scan (ϕ)) of TiN films tilted. The ϕ -scan results obtained from the same TiN film are displayed in Fig. 2. This figure also shows the ϕ -scan results of the sapphire substrate which has a hexagonal closed packed structure. The appearance of TiN film peaks and sapphire peaks, both spaced at 60° in the ϕ -scan, suggests the characteristics of 6-fold symmetry in both TiN and sapphire. However, the TiN film peaks have a phase difference of 30° with respect to peaking corresponding to the sapphire substrate. This phase difference is attributed to a rotation of the TiN plane with respect to substrate plane as shown schematically in Fig. 3. [34,35]. The 6-fold symmetry for TiN instead of an expected 3-fold symmetry for (111) oriented TiN film has been reported by numerous authors [34–36]. However, a clear explanation of this discrepancy has not been reported in the literature. The observation of a 6-fold symmetry rather than a 3-fold symmetry in (111) oriented TiN films is explained based on formation TiN grains with a twin structure, as shown schematically by regular and inverted triangles in Fig. 3. A possible TiN twin structure with epitaxial relationship with sapphire is: $(111)_{\text{TiN}}$ or $(\bar{1}\bar{1}\bar{1})_{\text{TiN}} \parallel (0001)_{\text{sapphire}}$. It can

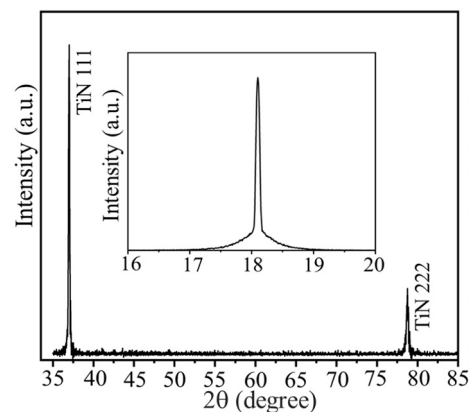


Fig. 1. X-ray diffraction pattern and Rocking curve of a TiN film grown on sapphire substrate at 773 K.

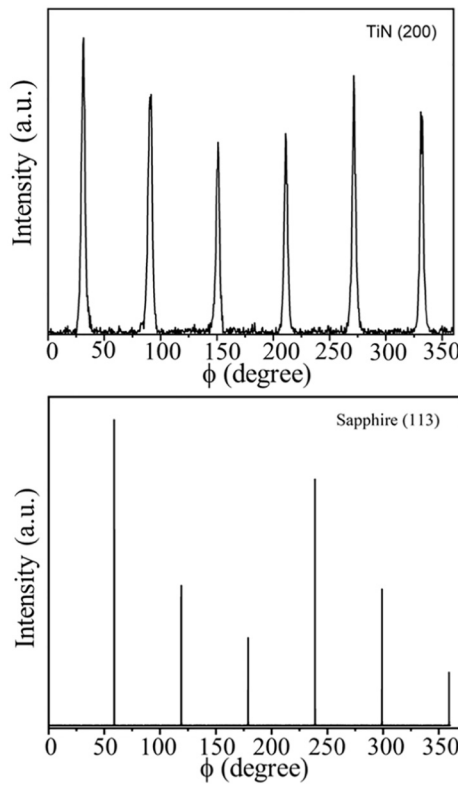


Fig. 2. Phi scan of TiN (200) and sapphire (113) planes.

be easily noted that the ϕ -scan peaks from TiN films are relatively wider than those from the single crystal sapphire substrate. The wider TiN peaks in the ϕ scan may be due to a possible disorder near the interface and defects in TiN films. This aspect in fact might be responsible for the higher resistivity values of our TiN film.

The variation of resistivity as a function of temperature for the epitaxially grown single crystalline TiN film on sapphire substrates is presented in Fig. 4 for magnetic flux density of 0, 0.5 and 1 T (1 T is equal to 1 Wb/m²). The $\rho(T)$ curves are separated into two regions as

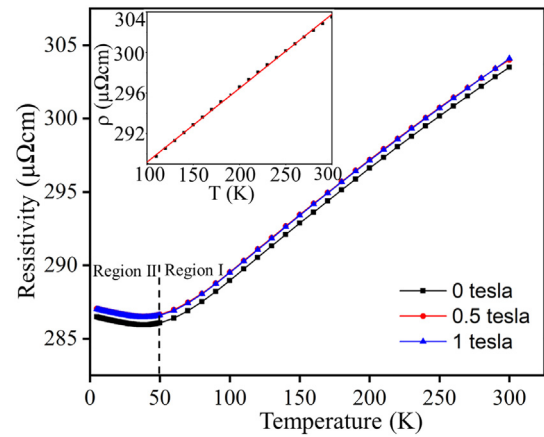


Fig. 4. Resistivity vs. Temperature in the temperature range of 10–300 K.

marked in Fig. 4: Region I where the resistivity decreases as the temperature decreases and Region II where the resistivity increases as the temperature decreases. The film shows a distinct minimum in resistivity (T_{min}) around 38 K in zero as well as in the presence of external magnetic fields. We have analyzed the $\rho(T)$ data at temperatures both above and below T_{min} . At higher temperatures, resistivity is determined by electron-phonon scattering and is linearly proportional to temperature in accordance to Eq. (1).

$$\rho(T) = \rho_0 + KT \tag{1}$$

where ρ_0 is the residual resistivity and K is a constant. As seen in the inset of Fig. 4, the zero field $\rho(T)$ data fit well to Eq. (1) in the temperature range of 100–300 K with a correlation coefficient of 0.9991 and a normalized χ^2 of $\sim 4 \times 10^{-6}$. Indeed, this is expected since the number of bosons (here phonons) is linearly proportional to temperature at higher temperatures. The normalized χ^2 has been defined as $(1/N)\sum_{i=1}^N [((\rho_{raw}^i - \rho_{fit}^i)^2)/\rho_{fit}^i{}^2]$ [37].

Since our primary interest was to study the $\rho(T)$ minima, we had measured ρ at very small temperature intervals as noted in Fig. 5. T_{min} , extracted from this figure and D_{min} , calculated using the expression: $D_{min} = [\rho(4K) - \rho(T_{min})]/\rho(4K)$, are plotted in Fig. 6 as a function of magnetic field applied. While T_{min} is clearly independent of the field

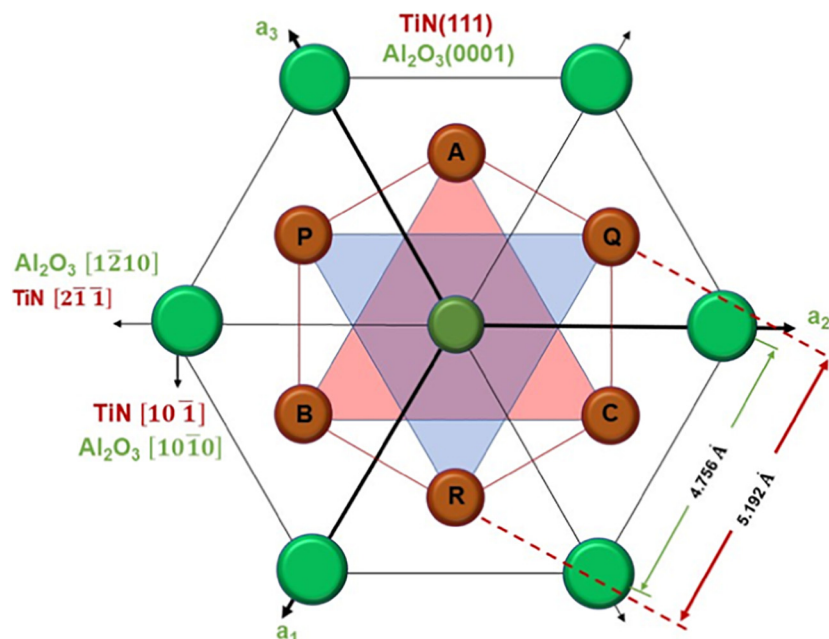


Fig. 3. Misorientation of TiN plane with respect to substrate plane.

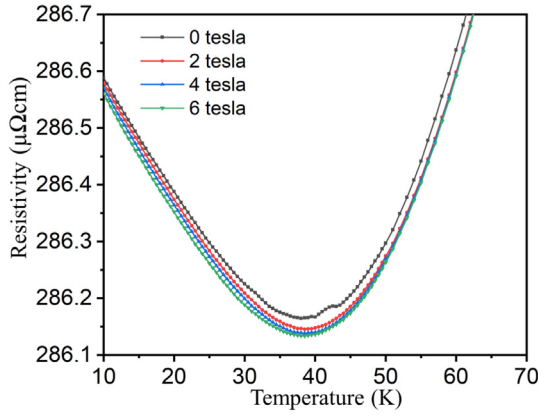


Fig. 5. Resistivity vs. Temperature near T_{\min} on an expanded scale.

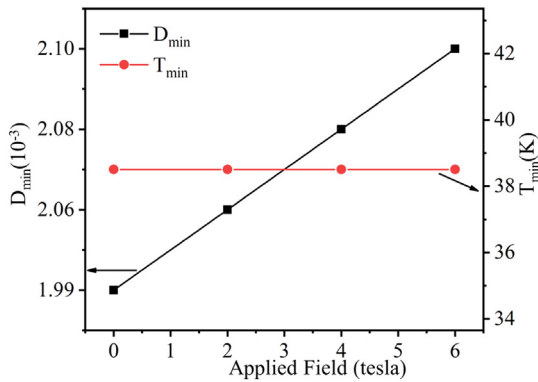


Fig. 6. T_{\min} and D_{\min} as functions of magnetic field.

applied, D_{\min} changes only by 5.25%, though almost linearly, as field changes from 0 to 6 T. The rise in resistivity in Fig. 5 below T_{\min} could be due to either the electron-electron (e - e) interaction via Eq. (2) or the Kondo effect via Eq. (3). Therefore, the high resolution $\rho(T)$ data were fitted to Eqs. (2) and (3).

$$\rho(T) = A + B\sqrt{T} \quad (2)$$

$$\rho(T) = C + D \ln(T), \quad (3)$$

where, A , B , C , and D are constants. As seen from the solid lines in Fig. 7a, the fit to Eq. (2) is excellent for the zero field $\rho(T)$ data with random deviation of the best-fitted curve from the data points in the entire temperature range ($4 \text{ K} \leq T \leq T_{\min}/2$). We have also analyzed the $\rho(T)$ data in other magnetic fields; the fits to Eq. (3) were found to be equally good as is evident from the values of the coefficients, their consistently small errors, and the normalized χ^2 of those fits, as listed in Table 1. Clearly, the \sqrt{T} fits are indeed excellent at all the fields. However, the fit to Eq. (3), as shown in Fig. 7b, is much less satisfactory as reflected from the systematic deviation of the best-fitted curve from the data points in the entire temperature range ($4 \text{ K} \leq T \leq T_{\min}/2$). The value of the normalized χ^2 in the $\ln(T)$ fit is also almost an order of magnitude larger (28×10^{-10}) when compared to the normalized χ^2 value (2.9×10^{-10}) in the \sqrt{T} fit (Table 1).

Thus, e - e interaction effect explains the low temperature data far more satisfactorily than Kondo effect. The field independence of T_{\min} (Fig. 6) also rules out the Kondo effect as a possible origin of resistance minima in TiN films because the Kondo effect is destroyed by magnetic fields.

In the weak-scattering limit Lee and Ramakrishnan [13] had shown that

$$\sigma(T) = \sigma_0 + m_\sigma \sqrt{T} \quad (4)$$

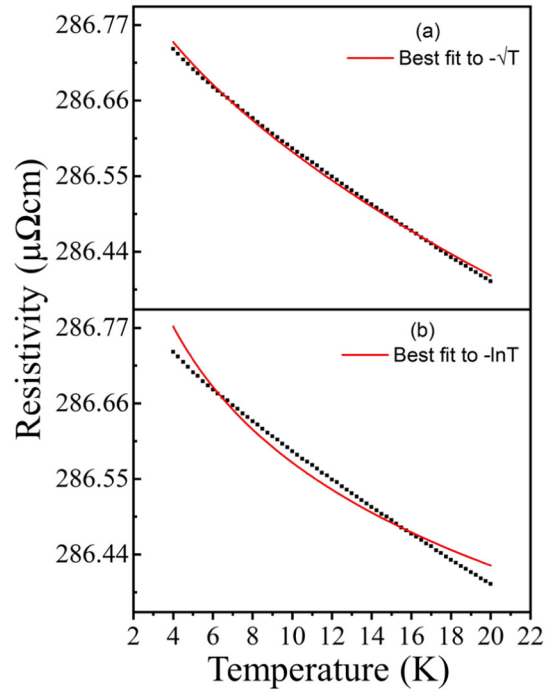


Fig. 7. Fits of Resistivity vs. Temperature at zero magnetic fields.

where m_σ can be expressed as.

$$m_\sigma = \frac{1.3e^2}{\pi^2 4\sqrt{2}\hbar} \left[\frac{4}{3} - \frac{3}{2} F_\sigma \right] \left[\frac{k_B}{\hbar D} \right]^{\frac{1}{2}}, \quad (5)$$

where F_σ is the screening constant for Coulomb interaction and D is the diffusion constant [38]. The zero-field $\rho(T)$ coefficient of the \sqrt{T} term, i.e. B in Eq. (2), in the film is $-0.137 \mu\Omega\text{cmK}^{-1/2}$. From this value of B , we have calculated the value of m_σ using Eq. (6):

$$m_\sigma = -B/A^2 \quad (6)$$

The value of m_σ was found to be $2 (\Omega\text{cmK}^{1/2})^{-1}$ which is of the same order of magnitude as that of a universal value of m_σ of $6 (\Omega\text{cmK}^{1/2})^{-1}$ and is also close to our earlier reported value of m_σ of $6.3 (\Omega\text{cmK}^{1/2})^{-1}$ [12] for nickel nanoparticles embedded on TiN films. Combining Eqs. (4) and (5) and assuming $F_\sigma = 0$, we have calculated the value of D to be $2.7 \text{ cm}^2/\text{s}$. Substituting this value of D in the Einstein equation, $\sigma = e^2 D N(E_F)$, $N(E_F)$ was found to be $\sim 4.7 \times 10^{46} \text{ J}^{-1} \text{ m}^{-3}$. This value of $N(E_F)$ compares well with $N(E_F)$ values of pure metals such as Au ($7.4 \times 10^{46} \text{ J}^{-1} \text{ m}^{-3}$) and Ti ($6.4 \times 10^{46} \text{ J}^{-1} \text{ m}^{-3}$). As discussed earlier, we find that quantum interference effects come into play in many kinds of materials with high resistivity. The interpretation of the resistance minima in terms of quantum interference effects is found to be independent of the nature of disorder that could be structural or compositional. It also does not depend on the magnetic state of the material.

4. Conclusions

Epitaxial and metallic TiN films were grown on sapphire substrates using a pulsed laser deposition method. Detailed electrical resistivity measurements have been carried out on those films in the temperature range of $4 \leq T \leq 300 \text{ K}$ at external magnetic fields from 0 to 6 T. At higher temperatures, the resistivity behavior was found to be linear in accordance with classical electron-phonon interactions ($\propto T$). Below the resistivity minima, the resistivity variation has been described very satisfactorily by the quantum interface effect ($\propto \sqrt{T}$) in the highly localized electrons in these high resistive TiN films. The value of the \sqrt{T} term coefficient of the electron-electron quantum interference matches well with the near-universal value.

Table 1Magnetic fields, values of the best-fitted parameters with their errors, normalized χ^2 , and correlation coefficient for fitting the data to Eqs. (2) and (3).

$\rho(T) = A + B\sqrt{T}$					$\rho(T) = C + D \ln(T)$			
H (T)	A ($\mu\Omega\text{cm}$)	B ($\mu\Omega\text{cmK}^{-1/2}$)	Normalized χ^2 (10^{-10})	Correlation coefficient	C ($\mu\Omega\text{cm}$)	D ($\mu\Omega\text{cm}$)	Normalized χ^2 (10^{-10})	Correlation coefficient
0	287.02 ± 0.03	−0.137 ± 0.001	2.9	0.9975	287.07 ± 0.01	−0.216 ± 0.004	28	0.9762
2	287.02 ± 0.02	−0.141 ± 0.002	1.8	0.9986	287.08 ± 0.01	−0.223 ± 0.004	25	0.9799
4	287.03 ± 0.02	0.147 ± 0.005	1.1	0.9992	287.09 ± 0.01	−0.233 ± 0.004	23	0.9829
6	287.04 ± 0.01	0.152 ± 0.003	0.4	0.9997	287.09 ± 0.01	−0.241 ± 0.004	21	0.9855

Acknowledgments

The authors would like to express thanks to the University of North Carolina (UNC) system for the seed funding via Interinstitutional Planning Grant (IPG) and Air Force Research Laboratory [Grant number FA8650-17-2-2229]. This work predominantly forms a part of the master's thesis of MR.

References

- R.V. Babinova, V.V. Smirnov, A.S. Useenov, K.S. Kravchuk, E.V. Gladkikh, V.I. Shapovalov, I.L. Mylnikov, Mechanical properties of titanium nitride films obtained by reactively sputtering with hot target, *J. Phys. Conf. Ser.* 872 (2017) 012035.
- H. Guo, W. Chen, Y. Shan, W. Wang, Z. Zhang, J. Jia, Microstructures and properties of titanium nitride films prepared by pulsed laser deposition at different substrate temperatures, *Appl. Surf. Sci.* 357 (2015) 473–478.
- M. Popović, M. Novaković, M. Mitrić, K. Zhang, N. Bibić, Structural, optical and electrical properties of argon implanted TiN thin films, *Int. J. Refract. Met. Hard Mater.* 48 (2015) 318–323.
- W.M. Mohammed, A.I. Gumarov, I.R. Vakhtov, I.V. Yanilkin, A.G. Kiiamov, S.S. Kharintsev, S.I. Nikitin, L.R. Tagirov, R.V. Yusupov, Electrical properties of titanium nitride films synthesized by reactive magnetron sputtering, *J. Phys. Conf. Ser.* 927 (2017) 012036.
- P. Jaipaan, C. Nannuri, N.R. Mucha, M.P. Singh, Z. Xu, A. Moatti, J. Narayan, S. Fialkova, R. Kotoka, S. Yarmolenko, O. Scott-Emuakpor, C. Binek, A. Kebede, D. Kumar, Influence of Gold Catalyst on the Growth of Titanium Nitride Nanowires, *Jaipaan, Panupong*, 7 (2018), pp. 720–725 (726).
- L. Li, A. Kishi, T. Shiraishi, Y. Jiang, Q. Wang, J.-P. Ao, Electrical properties of TiN on gallium nitride grown using different deposition conditions and annealing, *J. Vac. Sci. Technol. A* 32 (2014) 02B116.
- H.A. Smith, S. Elhamri, K.G. Eyink, L. Grazulis, M.J. Hill, T.C. Back, A.M. Urbas, B.M. Howe, A.N. Reed, Epitaxial titanium nitride on sapphire: effects of substrate temperature on microstructure and optical properties, *J. Vac. Sci. Technol. A* 36 (2018) 03E107.
- S. Vanapalli, K.L. Naidu, M.G. Krishna, K.A. Padmanabhan, Growth and mechanical properties of TiN-AuN₂ nanocomposite thin films on IN718 alloy substrates, *Mater. Lett.* 210 (2018) 101–104.
- P. Patsalas, N. Kalfagiannis, S. Kassavetis, Optical properties and Plasmonic performance of titanium nitride, *Materials* 8 (2015) 3128.
- F. Mehmood, R. Pachter, N.R. Murphy, W.E. Johnson, Electronic and optical properties of titanium nitride bulk and surfaces from first principles calculations, *J. Appl. Phys.* 118 (2015) 195302.
- S.C. Chen, K.Y. Sung, W.Y. Tzeng, K.H. Wu, J.Y. Juang, T.M. Uen, C.W. Luo, J.Y. Lin, T. Kobayashi, H.C. Kuo, Microstructure and magnetic properties of oxidized titanium nitride thin films in situ grown by pulsed laser deposition, *J. Phys. D: Appl. Phys.* 46 (2013) 075002.
- P. Khatua, T.K. Nath, M. Banerjee, A.K. Majumdar, Quantum interference effects and magnetic scattering in the electrical resistivity of Ni nanocrystallites in TiN matrix, *Appl. Phys. Lett.* 92 (2008) 193106.
- P.A. Lee, T.V. Ramakrishnan, Disordered electronic systems, *Rev. Mod. Phys.* 57 (1985) 287–337.
- S. Chakraborty, A.K. Majumdar, Hall effect in crystalline Ni-Fe-Cr alloys showing resistivity minima, *Phys. Rev. B* 57 (1998) 11850–11853.
- A.K. Majumdar, P.K. Khatua, K.D.D. Rathnayaka, D.G. Naugle, Correlation between the extraordinary hall constant and electrical resistivity minima in Co-rich metallic glasses, *Phys. Rev. B* 69 (2004) 214417.
- D. Kumar, J. Sankar, J. Narayan, R.K. Singh, A.K. Majumdar, Low-temperature resistivity minima in colossal magnetoresistive La_{0.7}Ca_{0.3}MnO₃ thin films, *Phys. Rev. B* 65 (2002) 094407.
- E. Babčí, R. Krsnik, C. Rizzuto, The impurity resistivity and resistivity minima in AlCr and AlMn alloys, *Solid State Commun.* 13 (1973) 1027–1030.
- J. Kondo, Resistance minimum in dilute magnetic alloys, *Prog. Theor. Phys.* 32 (1964) 37–49.
- Y. Katsuhiko, N. Kazuhiro, K. Tomohiko, M. Katsuhisa, O. Masami, Resistivities of titanium nitride films prepared onto silicon by an ion beam assisted deposition method, *J. Phys. D: Appl. Phys.* 37 (2004) 1095.
- L. Zude, Z. Guanghui, W. Xiaolin, Y. Minmin, Y. Bin, C. Xiang, Z. Weiping, L. Jingquan, Titanium nitride thin film for temperature sensing and its conductive mechanism in the cryogenic region, *Semicond. Sci. Technol.* 33 (2018) 115002.
- S.S. Rao, J.T. Prater, F. Wu, S. Nori, D. Kumar, J. Narayan, Integration of epitaxial permalloy on Si (100) through domain matching epitaxy paradigm, *Curr. Opin. Solid State Mater. Sci.* 18 (2014) 1–5.
- D. Kumar, A. Sarin, V. Verma, R. Venkatraman, Pulsed laser deposition assisted fabrication and characterization of Fe-Co nanoparticles embedded in TiN thin film matrix, *Thin Solid Films* 534 (2013) 561–565.
- A.K. Majumdar, Further evidence of electron–electron interaction in (Ni_{0.5}Zr_{0.5})_{1-x}Al_x amorphous alloys, *J. Magn. Mater.* 263 (2003) 26–31.
- B.L. Altschuler, A.G. Aronov, Fermi-liquid theory of the electron-electron interaction effects in disordered metals, *Solid State Commun.* 46 (1983) 429–435.
- P.A. Lee, Real-space scaling studies of localization, *Phys. Rev. Lett.* 42 (1979) 1492–1494.
- P.A. Lee, Localized states in a d-wave superconductor, *Phys. Rev. Lett.* 71 (1993) 1887–1890.
- P.A. Lee, T.V. Ramakrishnan, Magnetoresistance of weakly disordered electrons, *Phys. Rev. B* 26 (1982) 4009–4012.
- E. Šimánek, Origin of the resistivity minima in granular superconductors, *Phys. Rev. B* 25 (1982) 237–244.
- H.T. He, C.L. Yang, W.K. Ge, J.N. Wang, Resistivity minima and Kondo effect in ferromagnetic GaMnAs films, *Appl. Phys. Lett.* 87 (2005) 162506.
- W.J. de Haas, J. de Boer, G.J. van den Berg, The electrical resistance of gold, copper and lead at low temperatures, *Physica* 1 (1934) 1115–1124.
- W.J. De Haas, G.J. Van Den Berg, The electrical resistance of gold and silver at low temperatures, *Physica* 3 (1936) 440–449.
- L. Schubnikov, W.J. De Haas, A new phenomenon in the change of resistance in a magnetic field of single crystals of bismuth, *Nature* 126 (1930) 500.
- W.J. De Haas, J. De Boer, The electrical resistance of platinum at low temperatures, *Physica* 1 (1934) 609–616.
- D. Rasic, R. Sachan, M.F. Chisholm, J. Prater, J. Narayan, Room temperature growth of epitaxial titanium nitride films by pulsed laser deposition, *Cryst. Growth Des.* 17 (2017) 6634–6640.
- S.S. Yang, Y.R. Lin, S.T. Wu, Room temperature epitaxial growth of TiN on SiC, *Surf. Coat. Technol.* 201 (2007) 4850–4853.
- V. Talyansky, R.D. Vispute, R. Ramesh, R.P. Sharma, T. Venkatesan, Y.X. Li, L.G. Salamanca-Riba, M.C. Wood, R.T. Lareau, K.A. Jones, A.A. Iliadis, Fabrication and characterization of epitaxial AlN/TiN bilayers on sapphire, *Thin Solid Films* 323 (1998) 37–41.
- S. Chakraborty, A.K. Majumdar, Electron transport studies in Ni-rich γ -NiFeCr alloys, *J. Magn. Mater.* 186 (1998) 357–372.
- S. Chakraborty, A.K. Majumdar, Resistivity minima in concentrated γ -Cu_{100-x}Mn_x alloys (36 ≤ x ≤ 83), *Phys. Rev. B* 53 (1996) 6235–6239.